A PHYSICS BASED MODEL FOR ROTOR SYSTEM HEALTH MONITORING

Ranjan Ganguli* Inderjit Chopra †
Center for Rotorcraft Education and Research
Department of Aerospace Engineering
University of Maryland
College Park, MD 20742

David J. Haas ‡
Sea Based Aviation Office
Carderock Division
Naval Surface Warfare Center
Bethesda, MD 20084

Abstract

A physics based comprehensive model of the helicopter rotor in forward flight is used to analyze the impact of selected faults on rotor system behavior. The rotor model is based on finite elements in space and time. The faults modeled include freeplay in the pitch-control system and lag damper and friction in the flap and lag hinges and the pitch control system. In addition, the helicopter rotor model is used to develop a neural network based damage detection methodology. Simulated data from the rotor system is contaminated with noise and used to train a feedforward neural network using backpropogation learning. Cases considered for training and testing the neural network include both single and multiple faults on the damaged blade. Results show that the neural network can detect and quantify both single and multiple faults on the blade from noise contaminated simulated vibration and blade response test data. For accurate estimation of type and extent of damages, it is important to train the neural networks with noise contaminated response data. [1]

Nomenclature

C_d	blade section drag coefficient
C_l	blade section lift coefficient
C_m	blade section moment coefficient
C_T	thrust coefficient
d	damage level
e	error
e_{id}	error in damage identification
F	hub forces
F_x	longitudinal hub force
F_y	lateral hub force
F_z	vertical hub force
m	number of damage types
M	hub moments
M_x	rolling hub moment
M_y	pitching hub moment
M_z	yawing hub moment
N	number of spatial finite elements, number of damage levels for training data
N_b	number of blades
N_e	number of errors in damage detection
$\mathcal{N}$	neural network mapping
p	system response vector
P	input matrix for neural network
R	rotor radius
T	kinetic energy, target matrix for neural network
U	strain energy
v	lag deformation of blade
w	flap deformation of blade
W	virtual work
x	blade spanwise coordinate
δ	variation
α	angle of attack, noise level
Δ	difference between damaged and undamaged quantity
μ	advance ratio
σ	solidity ratio
ϕ	torsional deformation of blade, activation function
ψ	azimuth angle, time
Ω	rotation speed
$\angle$	change in phase angle
$()_{ic}$	ith cosine component
$()_{is}$	ith sine component
$()_n$	noise contaminated quantity
$()_{test}$	related to test data
$()_{tr}$	related to training data

*Assistant Research Scientist
†Professor and Director
‡Aerospace Engineer
[1]Presented at the 22nd European Rotorcraft Forum, 16-19 September 1996, Brighton, UK

$()_0$ zeroth harmonic, steady quantity

Introduction

Helicopter rotors are subject to high vibratory forces because of highly flexible rotating blades and a severe aerodynamic environment. This leads to wear in various components of the rotor, requiring frequent inspection and replacement of damage sensitive components leading to high maintenance costs. In fact, maintenance costs account for about a quarter of the direct operating costs of rotorcraft [1]-[2]. Health and usage monitoring systems (HUMS) can reduce this cost. The helicopter industry has recently focussed on HUMS to provide fault diagnosis for drivetrain, engines, oil system and rotor system [3]-[4]. Current track and balance systems can detect rotor faults to a limited extent. For example, when track and balance adjustments do not alleviate a high vibration problem, a faulty component may be indicated. To develop a health monitoring system for a rotor, the relationship between blade damage and helicopter system behavior is needed. Since it is difficult to obtain flight test data for a damaged helicopter rotor, a physics based model offers the opportunity to study the simulated behavior of the damaged helicopter. Numerical simulations of the damaged rotor system response can be used by artificial intelligence based techniques such as neural networks to learn the relationship between rotor faults and system behavior. The trained neural network can then be placed online on the helicopter to detect and identify damage from rotor vibration and response data.

The fault detection methodology approach discussed above focuses on global faults. Global faults are those which can be detected using remote measurements of "global" system parameters such as fuselage vibration and blade deflection. The theoretical basis of global fault detection is that for an undamaged rotor all blades will have identical response and only the N/rev loads will be transmitted to the hub by a N-bladed rotor. If however, one blade is dissimilar to the other blades due to a fault then all harmonics of the rotor loads are transmitted to the hub. In addition, the response of the damaged blade will be different from the undamaged blades.

Selected works on global fault simulation has been reported in the literature [5]-[7]. Azzam and Andrew [5] simulated rotor system faults for a five bladed articulated rotor similar to the S-61 rotor using a computer based math-dynamic model. Faults modeled include blade cracks, chordwise mass imbalance and defective lag damper. The present authors [6]-[7] have applied a comprehensive aeroelastic analysis based on finite element in space and time to simulate a damaged rotor. Numerical results were obtained in hover and in forward flight for an articulated four bladed rotor similar to the SH-60 rotor. Selected predictions of rotor component loads were validated with flight test data [6]. Faults modeled in Ref. [6] include moisture absorption, loss of trim mass, damaged pitch-control system, defective lag damper, damaged trim tab and misadjusted pitch-link. Faults modeled in Ref. [7] include aerodynamic mistracking, blade crack, stiffness defect, manufacturing defect and chordwise mass imbalance. The influence of simulated rotor faults on blade response and vibratory hub loads was analyzed and summarized in the form of diagnostic charts. It was concluded that most rotor faults can be detected by monitoring blade response and vibration. However, localized damage such as blade cracks are difficult to detect from global system behavior.

The above studies focussed on calculation of rotor response due to simulated rotor system faults. However, there is a need to use the simulated data to develop a fault detection methodology. Addressing this issue, the present authors [9] developed a neural network based approach for rotor system fault detection. Two neural networks were used; the first network to classify the type of fault and the second network to characterize the level of damage. The neural networks are trained from a numerically generated rotor system fault database. One drawback of a neural network trained with ideal data is that it classifies ideal test data exactly but gives significant errors when noise is added to the test data. This problem was overcome by adding noise to the analytical simulation during training. A fault detection system based on noisy simulated data was found to be more robust than that developed using ideal simulated data because it accounts for the inherent uncertainty in the real system. Testing of the trained neural network showed that it can detect and identify damage in the rotor system from simulated blade response and vibration data.

In addition to global faults such as those discussed above, there are local faults which are difficult to detect from global system behavior such as fuselage vibration and rotor response[11]. Localized structural damage such as blade cracks and delamination are examples of local faults. Undetected blade cracks can lead to catastrophic failure depending on crack location, flight conditions and load severity. Local fault detection methods have evolved to detect such faults. The methods used for local fault detection include robust laser interferometer, photoelastic techniques, ul-

trasonic techniques and acoustic emission sensors [10]. Such local fault detection techniques complement the global fault detection approach discussed in this paper. When combined together, they can form a comprehensive approach to rotor system health monitoring.

Rotor system health monitoring remains a very challenging area for research because of the complexity of the rotor. For example, pilot control inputs to the rotor blades are transmitted by a series of connecting rods, linkages, swashplates, pushrods and control horns. These components are exposed to wear and tear which can lead to jamming and misalignment/freeplay. Also, the rotor blades are attached to the hub via a series of components that include bearings, pins, tie rods and spindles. Again, there is the possibility of jamming or freeplay in these components due to wear and tear. In this paper, the faults discussed include friction in hinges and pitch-control system and freeplay in the pitch-control system and in the lag damper. Physics based models are developed for each fault and their influence on rotor system behavior are identified.

The damage detection techniques discussed in previous research focussed on primary faults (only one type of fault on the blade) [9]. In this paper, the detection of compound faults is addressed. Compound faults involve more that one type of fault on the damaged blade. Detecting the components with a compound fault is important for distinguishing between benign faults (such as track and balance problems) and potentially catastrophic faults (such as damaged lag damper).

Formulation

Mathematical Model of Rotor-System

The helicopter is represented by a nonlinear model of several elastic rotor blades dynamically coupled to a six degree of freedom rigid fuselage. Each blade undergoes flap bending, lag bending, elastic twist and axial displacement. Formulation is based on a generalized Hamilton's principle applicable to nonconservative systems:

$$\int_{\psi_1}^{\psi_2} (\delta U - \delta T - \delta W) d\psi = 0 \qquad (1)$$

The δU, δT and δW are virtual strain energy, kinetic energy and virtual work, respectively. The δU and δT also include energy contributions from components which are attached to the blade, e.g., pitch link, lag damper etc. External aerodynamic forces on the rotor blade contribute to the virtual work variational, δW. For the aeroelastic analysis, aerodynamic forces and moments are calculated using an inflow distribution from the Scully-Johnson free wake model [12] and unsteady effects are accounted for using the Leishman-Beddoes model [13].

Finite element methodology is used to discretize the governing equations of motion, and allows for accurate representation of complex hub kinematics and nonuniform blade properties. After finite element discretization, Hamilton's principle is written as

$$\int_{\psi_i}^{\psi_f} \sum_{i=1}^{N} (\delta U_i - \delta T_i - \delta W_i) d\psi = 0 \qquad (2)$$

Each beam element has fifteen degrees of freedom. These degrees of freedom correspond to cubic variations in axial elastic and (flap and lag) bending deflections and quadratic variation in elastic torsion.

The first step in the aeroelastic analysis procedure is to trim the vehicle for the specified operating condition. The blade finite element equations are transformed to normal mode space for efficient solution of the blade response. The nonlinear, periodic, normal mode equations are then solved for steady response using a finite element in time method. Steady and vibratory components of the rotating frame blade loads (i.e. shear forces and bending/torsion moments) are calculated using the force summation method. In this approach, blade aerodynamic and inertia forces are integrated directly over the length of the blade. Fixed frame hub loads are calculated by summing the contributions of individual blades. A coupled trim procedure is carried out to solve for the blade response, pilot input trim controls, and vehicle orientation, simultaneously. The coupled trim procedure is essential for elastically coupled blades since elastic deflections play an important role in the steady net forces and moments generated by the rotor.

Modeling of Rotor-System Faults

The faults modeled in this paper are shown in Table 1 and are discussed below.

Freeplay in Pitch Control System

The pitch-control system is exposed to severe loading conditions which can cause wear and looseness leading to freeplay. Freeplay in the pitch-control system is modeled by the nonlinear spring whose characteristics are shown in Fig. 1. For the undamaged blade, the pitch-link load varies linearly with displacement and the pitch-link stiffness is

Table 1: Potential Rotor Head Damage

Type of damage	Simulation of Damage
Freeplay in Pitch Control System	Nonlinear Spring
Freeplay in Lag Damper	Nonlinear Damper
Friction in Lag Hinge	Coulomb Damping
Friction in Flap Hinge	Coulomb Damping
Friction in Pitch Control System	Coulomb Damping

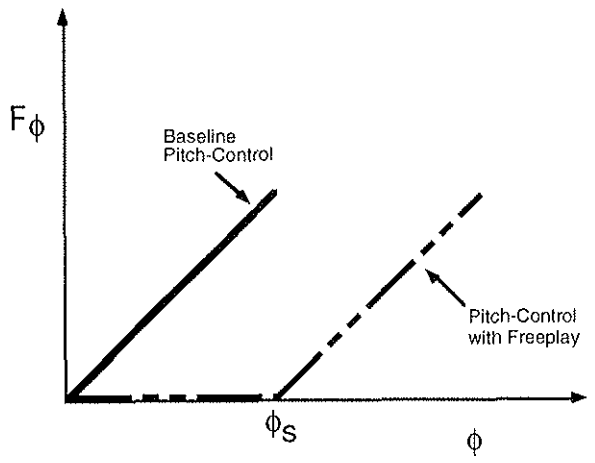

Figure 1: Schematic representation of pitch-link load for blade with freeplay in pitch-control system

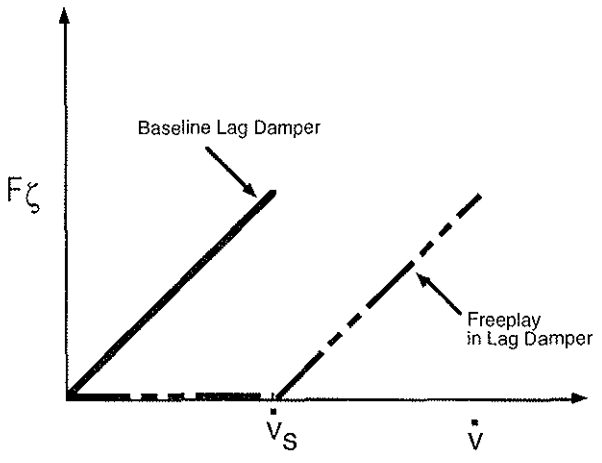

Figure 2: Schematic representation of lag damper load for blade with freeplay in lag damper

K_ϕ. However, for the blade with freeplay in the pitch-control system, the pitch-link stiffness is zero unless the torsion displacement exceeds a value ϕ_s, thereafter, the stiffness is K_ϕ.

$$\begin{aligned} F_\phi &= 0 \ for \ \phi < \phi_s \\ &= K_\phi(\phi - \phi_s) \ for \ \phi \geq \phi_s \end{aligned} \quad (3)$$

Freeplay in Lag Damper The lag dampers used for articulated rotors are typically hydraulic dampers. These dampers have linear characteristics for most of their operating conditions. Sloppiness in the lag damper may cause the damper to loose its effectiveness at low values of lag velocity. This is modeled by the damper whose characteristics are shown in Fig. 2. For the undamaged blade, the damper load varies linearly with lag velocity and the damping value is C_ζ. However, for the blade with freeplay in the lag damper, the damping is zero unless the lag velocity exceeds a value $\dot{v}_s$, thereafter, the damping is C_ζ. In mathematical form the damper force is:

$$\begin{aligned} F_{ld} &= 0 \ for \ \dot{v} < \dot{v}_s \\ &= C_\zeta(\dot{v} - \dot{v}_s) \ for \ \dot{v} \geq \dot{v}_s \end{aligned} \quad (4)$$

Friction in Hinges and Bearings Coulomb friction damping is used to model friction at hinges or bearing caused by lack of lubrication or wear. The equations of motion for the baseline rotor blade without any friction damping can be written as

$$M\ddot{q} + C\dot{q} + Kq = F \quad (5)$$

When additional friction damping is added to the system, the equations become:

$$M\ddot{q} + C\dot{q} + \mu\frac{\dot{q}}{|\dot{q}|} + Kq = F \quad (6)$$

where μ is a measure of Coulomb friction damping in the system. Three cases are considered: friction in the flap hinge, friction in the lag hinge and friction in the pitch-control system.

Indicators of System Damage

It is assumed that one blade is damaged and the other blades are undamaged. For the undamaged rotor (assuming perfectly tracked blades), all 4-blades will have identical tip response (magnitude and phase). Also, for a perfectly tracked rotor, only 4/rev and 8/rev forces and moments will be transmitted by the undamaged rotor to the fuselage.

In practise, however, there will always be some level of fuselage response at 1/rev and at higher harmonics due to the inability to perfectly balance and track a rotor. Typically, a 1/rev fuselage response of 0.15 inch per second (ips), equivalent to about 170 lb, is representative of a well balanced rotor. Vibrations in excess of 0.30 ips are considered significant and indicate the need to track and balance the rotor. Approximate thresholds for the moments transmitted to the fuselage can be similarly obtained. Moments below 2500 lb-in are representative of a well tracked and balanced rotor. Moments above 5000 lb-in indicate the need to track and balance the rotor.

Similarly, for the blade tip response, most real rotors display some degree of variation in tip displacements between blades even when the rotor is considered to be in a 'tracked' condition. In this study, we assume that variations in tip deflections less than a quarter of an inch are negligible, and changes in elastic twist of less than a quarter of a degree are considered too small to be of practical value. These measures for system response are shown in Table 2.

The vibratory hub loads and blade response predicted by the math-model are assembled into the following vector form:

$$p = \lfloor \Delta v \ \Delta w \ \Delta\phi \ F_x \ F_y \ F_z \ M_x \ M_y \ M_z \rfloor^T \qquad (7)$$

Blade response harmonics greater than 5 and load harmonics greater than 10 are very small and are neglected. The change in blade tip response between the damaged and undamaged blade is expressed in the form (for flap response):

$$\begin{aligned} \Delta w \ = \ & \lfloor \Delta w_0 \ \Delta w_{1c} \ \Delta w_{1s} \ \Delta w_{2c} \ \Delta w_{2s} \\ & \Delta w_{3c} \ \Delta w_{3s} \ \Delta w_{4c} \ \Delta w_{4s} \ \Delta w_{5c} \ \Delta w_{5s} \rfloor^T \end{aligned} \qquad (8)$$

The blade lag and torsion response can be similarly expressed. The vector for the longitudinal force is given as

$$\begin{aligned} F_x \ = \ & \lfloor F_{x0} \ F_{x1c} \ F_{x1s} \ F_{x2c} \ F_{x2s} \ F_{x3c} \ F_{x3s} \\ & F_{x4c} \ F_{x4s} F_{x5c} \ F_{x5s} \ F_{x6c} \ F_{x6s} \ F_{x7c} \ F_{x7s} \\ & F_{x8c} \ F_{x8s} \ F_{x9c} \ F_{x9s} \ F_{x10c} \ F_{x10s} \rfloor^T \end{aligned} \qquad (9)$$

Similar vectors define the other forces and moments. The vector p in Eq. 7 has 159 elements and contains the needed information about the damaged rotor system in mathematical form.

To simulate data contaminated by noise, zero-mean white noise with a normal distribution is added to p. The noise is added to each element of the p vector as follows:

$$p_{ni} = p_i + p_i \alpha\epsilon = p_i(1 + \alpha\epsilon) \qquad (10)$$

where ϵ is a random number between -1 and 1 from the normal distribution and α is the noise level. A value of α of 0.05 is refered to as five percent noise and implies an uncertainty of 5 percent in the data for p_i. The noisy response vector is denoted by p_n.

Neural Network Architecture

Two neural networks are used for the damage detection problem. Both networks consists of an input layer, a hidden layer and an output layer. A schematic of the network is shown in Fig. 3. The first network (called Network A) is a pattern classifier. Network A determines the type (or types) of damage, for example, whether the damage is moisture absorption or a defective lag damper, or a combination of both. For Network A, the hidden layer and the output layer consist of nonlinear logarithmic sigmoid neurons, an architecture known to be suitable for pattern classification [14]. These neurons use sigmoid activation functions of the type:

$$\phi(v) = \frac{1}{1 + exp(-v)} \qquad (11)$$

The second network (called Network B) is a function approximator. For Network B, the hidden layer consists of nonlinear log-sigmoid neurons and the output layer consist of linear neurons, an artitecture known to be suitable for function approximation problems. Network B assumes that Network A has isolated the type of damage, and uses this information to determine the magnitude of damage. This procedure is shown schematically in Fig. 4.

A backpropagation algorithm with added momentum and an adaptive learning rate is used [15]. The error measure of the networks is defined as

$$e_k = \frac{||t - t'_k||}{||t||} \qquad (12)$$

where t is the desired target vector and t'_k is the output vector produced by the network at the end of the kth iteration and where $||.||$ is the Euclidean norm. The algorithm is assumed to have converged when the error becomes sufficiently small ($e_k = 0.00001$).

Table 2: Quantitative Measures for System Behavior

Measure (units)	Tip flap, lag (inch)	Tip torsion (degrees)	Forces (lb)	Moments (lb-in)	Phase (degrees)	Symbols
Negligible	< 0.25	< 0.25	< 170	< 2500	< 10	$\sim$
Moderate	0.25-0.50	0.25-0.50	170-340	2500-5000	10-30	$\circ$
Significant	>0.50	>0.50	>340	>5000	>30	$\bigcirc$

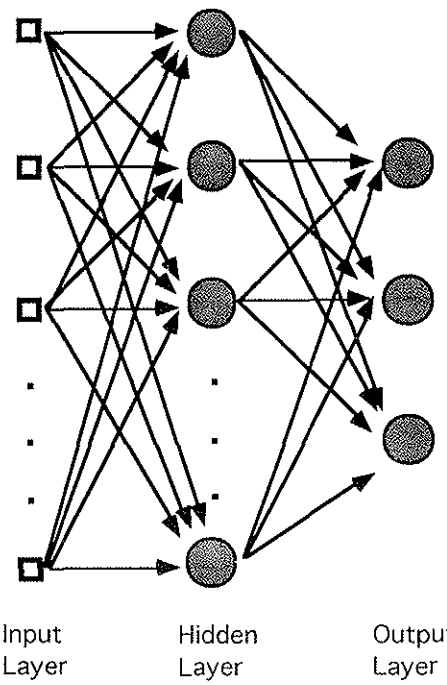

Figure 3: Schematic representation of multi-layer neural network

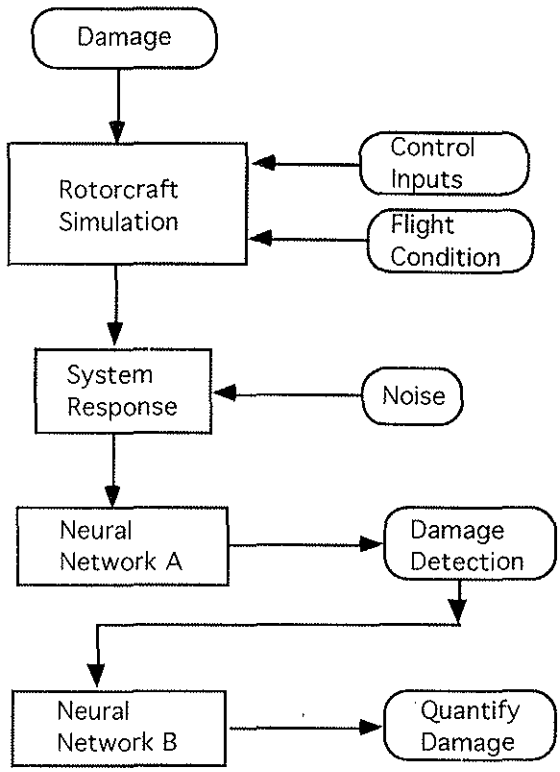

Figure 4: Schematic representation of model based damage detection procedure

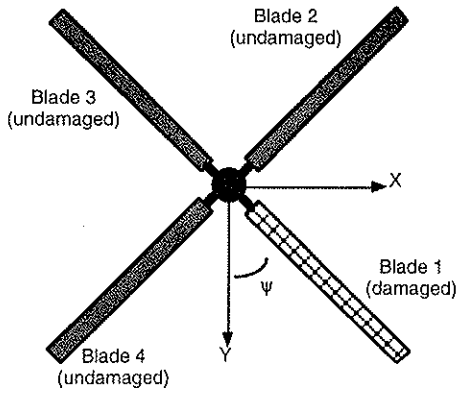

Figure 5: Schematic representation of damaged blade

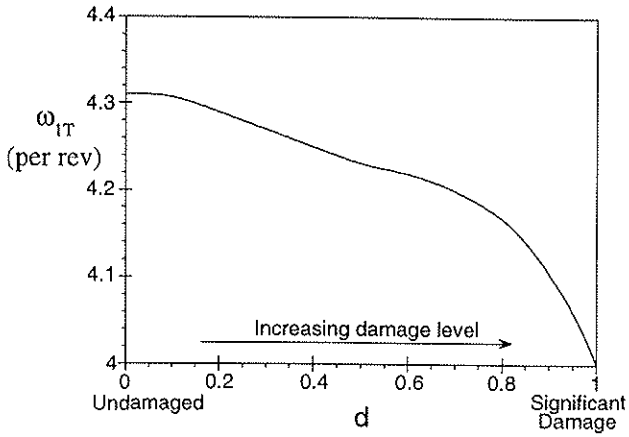

Figure 6: First rotating torsion frequency of blade with damaged pitch-control system

Training Database

Three representative rotor faults are used to train the neural network: moisture absorption, defective lag damper and damaged pitch-control system. In each case, training data are generated by starting with an undamaged rotor and progressively increasing the damage intensity on Blade 1 (see Fig. 5).

The training target vectors are defined as:

$$d = [0 \;\; 0.1 \;\; 0.2 \;\; \ldots \;\; 0.9 \;\; 1.0] \qquad (13)$$

The value 0 corresponds to the undamaged case and 1.0 corresponds to significant damage. Intermediate values of d represents a linear variation in the damage magnitude between these extremes. For moisture absorption, $d_i = 1$ corresponds to an increase in mass of the damaged blade by 3 percent, compared to the undamaged blade. For the defective lag damper, $d_i = 0$ corresponds to a lag damping constant $C_\zeta = 3000$ lb sec/in, and $d_i = 1$ corresponds to a lag damper constant C_ζ of the damaged blade equal to zero. For the pitch-control system, damage level is represented by a linear reduction in pitch-link stiffness from 100 percent for the undamaged blade to 12 percent for the damaged blade. This corresponds to a reduction in the baseline torsion frequency from 4.31 per rev for the undamaged blade ($d_i = 0$) to 4.0 per rev for the damaged blade ($d_i = 1$). The variation of the first torsion mode frequency with pitch-control system damage level is shown in Fig. 6. The aeroelastic analysis is performed for the values of d defined above and for each case the system response vector p defined by Eq. 7 is calculated. These data form the simulated fault database. The database is divided into two parts depending on the value of d. One part is used for training the neural network (Eq. 14), and the other for testing the trained neural network (Eq. 15).

$$d_{tr} = [0 \;\; 0.2 \;\; 0.4 \;\; 0.6 \;\; 0.8 \;\; 1.0] \qquad (14)$$

$$d_{test} = [0.1 \;\; 0.3 \;\; 0.5 \;\; 0.7 \;\; 0.9] \qquad (15)$$

For each damage type,six damage levels used for training and five damage levels used for testing. When there is more than a single fault on the damaged blade, the data needed for training the neural network becomes large as the number of faults increases. For example, for two faults on the damaged blade, there are 36 (NxN) combinations of damage levels for training and 25 (5x5) for testing the neural network.

Damage Detection

Neural Network A is used for damage detection. The input to the neural network is the vector p, defined at N damage levels (Eq. 14), for the three damages being considered. The input matrix P is given as

$$P = [P_1 \;\; P_2 \;\; P_3 \;\; P_{12} \;\; P_{13} \;\; P_{23}] \qquad (16)$$

where

$$\begin{aligned} P_1 &= [p_1 \; p_2 \; \ldots p_N] \quad \textit{for damage 1} \\ P_2 &= [p_1 \; p_2 \; \ldots p_N] \quad \textit{for damage 2} \\ P_3 &= [p_1 \; p_2 \; \ldots p_N] \quad \textit{for damage 3} \end{aligned}$$

Each matrix P_k shown above has 159 rows and N columns and represents a single fault on the damaged blade. For the case with two faults on the damaged blade, the input matrices are

$$P_{12} = \begin{bmatrix} p_{11} \; p_{12} \; \cdots p_{1N} \\ p_{21} \; p_{22} \; \cdots p_{2N} \end{bmatrix}$$

$$\vdots \quad (17)$$

$$p_{N1}\ p_{N2}\ \cdots\ p_{NN}]$$

for damage 1 *and* 2

$$P_{13} = [p_{11}\ p_{12}\ \cdots p_{1N}$$

$$p_{21}\ p_{22}\ \cdots p_{2N}$$

$$\vdots \quad (18)$$

$$p_{N1}\ p_{N2}\ \cdots\ p_{NN}]$$

for damage 1 *and* 3

$$P_{23} = [p_{11}\ p_{12}\ \cdots p_{1N}$$

$$p_{21}\ p_{22}\ \cdots p_{2N}$$

$$\vdots \quad (19)$$

$$p_{N1}\ p_{N2}\ \cdots\ p_{NN}]$$

for damage 2 *and* 3

(20)

Each matrix P_{ij} has 159 rows and $N \times N$ columns. The element p_{ij} represent the system response vector p for two damages at damage levels i and j. In each case, i and j range from 1 to N. The target vector T is given as

$$T = \begin{bmatrix} \lfloor 1 \rfloor & \lfloor 0 \rfloor & \lfloor 0 \rfloor & \lfloor 1 \rfloor & \lfloor 1 \rfloor & \lfloor 0 \rfloor \\ \lfloor 0 \rfloor & \lfloor 1 \rfloor & \lfloor 0 \rfloor & \lfloor 1 \rfloor & \lfloor 0 \rfloor & \lfloor 1 \rfloor \\ \lfloor 0 \rfloor & \lfloor 0 \rfloor & \lfloor 1 \rfloor & \lfloor 0 \rfloor & \lfloor 1 \rfloor & \lfloor 1 \rfloor \end{bmatrix} \quad (21)$$

where

$$\lfloor 1 \rfloor = \{1\ 1\ \ldots 1\} \quad (22)$$

$$\lfloor 0 \rfloor = \{0\ 0\ \ldots 0\} \quad (23)$$

Here $\lfloor 1 \rfloor$ and $\lfloor 0 \rfloor$ are row vectors of size N or size $N \times N$ depending on the nature of the fault (primary or compound). The row in which 1's are present in the T matrix correspond to the type of damage. The neural network performs a mapping of training vector P into target vector T and can be written as

$$T = \mathcal{N}(P) \quad (24)$$

where $\mathcal{N}$ is the neural network mapping. The effect of noise is included by defining an augmented training matrix

$$P_n = \lfloor P\ \ P\ \ P'\ \ P'' \rfloor \quad (25)$$

where P' and P'' are noise contaminated signals defined as $(P')_i = (P)_i + (P)_i\ 0.05\epsilon$ and $(P'')_i = (P)_i + (P)_i\ 0.1\epsilon$ represent 5 percent and 10 percent noise contamination, respectively. The augmented training matrix contains two copies of the ideal matrix and two noisy matrices. These inputs are all matched to the same target outputs. The augmented target vector is obtained as

$$T_n = \lfloor T\ \ T\ \ T\ \ T \rfloor \quad (26)$$

The network mapping with noisy data can now be represented as

$$T_n = \mathcal{N}_n(P_n) \quad (27)$$

For each fault, the pattern from only ideal data is expanded by adding noise contaminated data. The neural network is trained to map these patterns with the faults causing them. For training the network, the following procedure is followed. First, the network is trained using ideal data as shown in Eq. 24. Next, the network is trained on noisy data for ten cycles, as shown in Eq. 27. For each training cycle, the converged weights are used as the starting values from the previous cycle. For each cycle, a different randomly generated seed value is used by the random number generator to form the noisy data. The ten cycles provide considerable noisy training data and generalizes the input patterns mapping onto the faults. Finally, to ensure that the network recognizes the ideal vectors, it is again trained on ideal data. The training of the network on several samples of noisy data increases generalization capability and makes the network more robust [17].

It is clear that the above procedure can be expanded to include a higher amount of noise by further augmenting the training and target matrices with noisy data. This method of training using augmented matrices is known as *batch* training in contrast to *pattern* training where the inputs are given sequentially to the network. Utilizing *batching* operation is often more efficient and provides a more accurate estimate of the gradient vector used in backpropagation [14].

Damage Identification

Neural Network B is used for damage identification. The input to the neural network is the matrix P corresponding to the damage (or damages) detected by Network A. A seperate network is used for each damage type. Once the type of damage is known, the problem is to determine the extent of damage. The target vector is defined in Eq. 14 for a single fault. For a compound fault, the target vector is a combination of the damage levels defined by Eq. 14. For example, for Damage k, the neural network is trained for the following mapping:

$$d_{tr} = \mathcal{N}(P_k) \quad (28)$$

The issue of noisy data is also addressed for the damage identification network. This is done by defining the augmented matrix

$$P_{k_n} = \lfloor P_k\ \ P_k\ \ P'_k\ \ P''_k \rfloor \quad (29)$$

and the augmented target vector

$$d_{tr_n} = \lfloor d_{tr}\ \ d_{tr}\ \ d_{tr}\ \ d_{tr} \rfloor \quad (30)$$

Table 3: Helicopter Properties

Rotor Radius	26.8 ft
Flap and Lag Hinge Offset	15 in
Number of Blades	4
Blade Chord	20.76 in
Linear Aerodynamic Twist	-18^o
C_l	6.0 α
C_d	.002 + .2 α^2
C_m	0.0
Lock Number	8.00
Solidity	.0826
Blade Attachment Point	41.5 in
Rotor Tip Speed	725 ft/sec
Helicopter Weight	16500 lb
Blade Mass	235 lb

where P'_k and P''_k are noisy signals generated using 5 percent and 10 percent noise contamination, respectively. The network mapping with noisy data is therefore given as

$$d_{tr_n} = \mathcal{N}_n(P_{k_n}) \tag{31}$$

Again, the ideal and noisy vectors have the same input targets. The network is first trained using ideal data (Eq. 28), then trained using ten cycles of noisy data (Eq. 31), and finally trained with ideal data again.

Results and Discussion

For results, a 4-bladed articulated rotor with properties similar to a SH-60 helicopter is selected (see Table 3). The rotor blade is modeled using thirteen spatial finite elements along the bladespan (Fig. 7). Six time finite elements with fourth order shape functions are used along the azimuth to calculate the blade response. The results are obtained for a normalized rotor thrust coefficient $C_T/\sigma = 0.0726$ and a rotor advance ratio of $\mu = 0.3$. Selected validation of rotor component loads using this simulation for a baseline configuration are provided in Ref. [7].

Damaged Rotor System Behavior

The baseline flap and lag response of the undamaged rotor is shown in Fig. 8. The lag response has a predominant 1/rev component and the flap response has a 1/rev and 2/rev component. The baseline elastic twist of the undamaged rotor is shown in Fig. 9. The torsion response has a significant 1/rev component. For numerical results with a freeplay in the pitch control system ϕ_s of 0.15 degree is used (Eq. 3). This is about half of

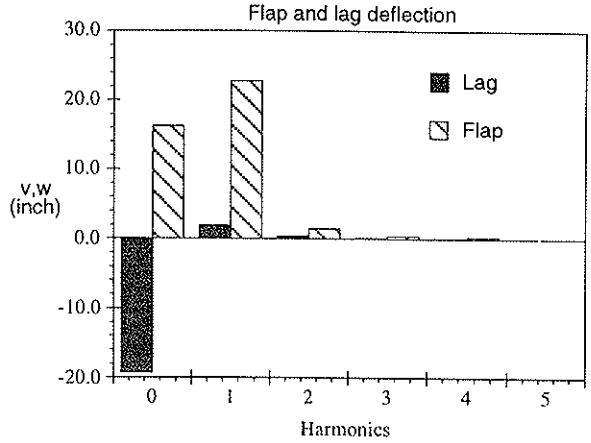

Figure 8: Flap and lag deflection for undamaged blades

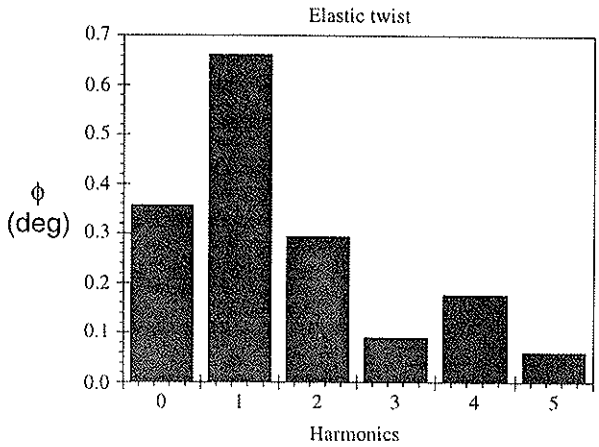

Figure 9: Elastic twist for undamaged blades

the steady elastic twist. For freeplay in the lag damper $\dot{v}_s$ is equal to half the 1/rev lag velocity (eq. 4). For friction, a value of $\mu = 300$ is used (Eq. 6).

The harmonic content of the difference in blade response between the undamaged and damaged blade is shown in Figs. 10-12. For an undamaged blade the difference is response of the four blades is zero. The information in these figures is summarized in the diagnostic chart (Table 4). The symbols used in the diagnostic table is defined in Table 2 and the '+' and '-' signs in the diagnostic tables refer to an increase or decrease in the given quantity, respectively. Freeplay in the pitch-control system causes a moderate increase in the 1/rev flap deflection of the damaged blade and a moderate decrease in the 2/rev elastic twist.

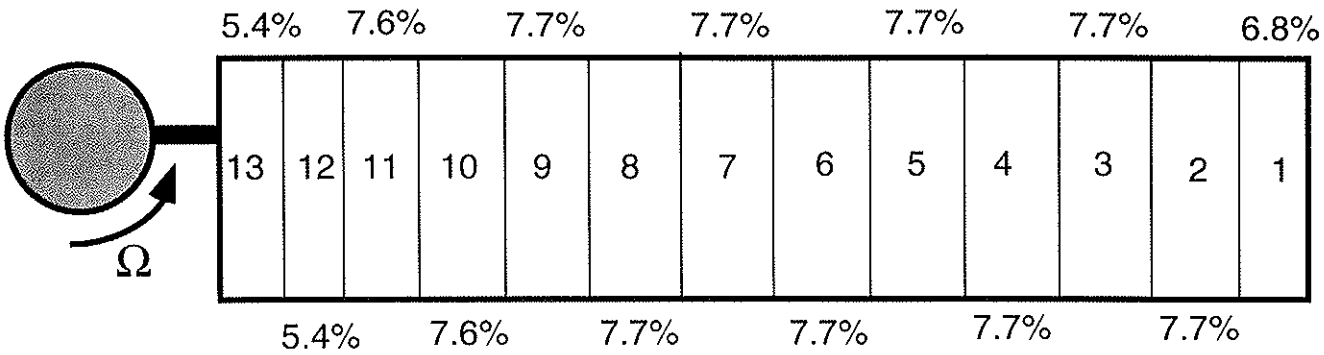

Figure 7: Finite element model of rotor blade (element length shown in percent span)

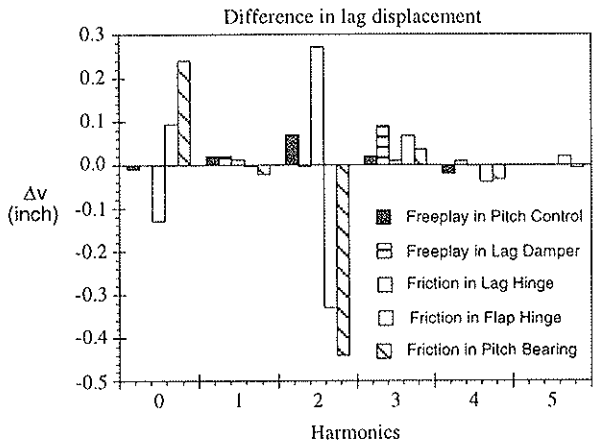

Figure 10: Difference in lag deflection between undamaged and damaged blades

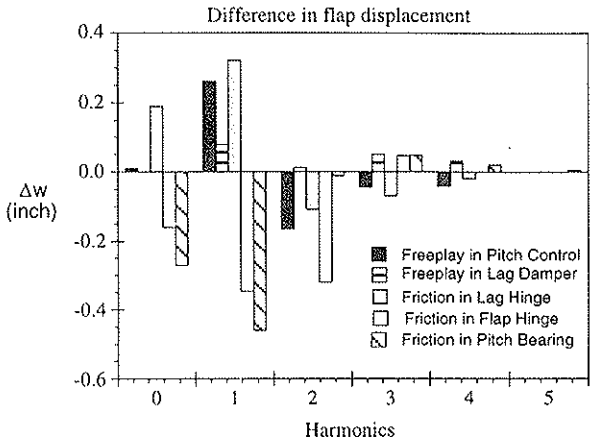

Figure 11: Difference in flap deflection between undamaged and damaged blades

Freeplay in the lag damper causes a moderate increase in the 1/rev elastic twist. Friction in the lag hinge causes a moderate increase in the 2/rev lag response and the 1/rev flap response. Friction in the flap hinge causes a moderate decrease in the 2/rev lag response, an increase in the 1/rev flap and torsion response and a decrease in the 2/rev flap response. Friction in the pitch bearing causes a moderate reduction in the 2/rev lag response and the steady and 1/rev flap response.

The harmonic content of the hub loads of the undamaged and damaged rotor are shown in Figs. 13-18. The first four and the eighth harmonic are shown in these figures. The fifth, sixth and seventh harmonics are negligible for the damages considered and are not shown. For an undamaged rotor, only the 4/rev and 8/rev harmonics are transmitted by the rotor to the fuselage. The information about hub forces in these figures is summarized in Table 5. The effect of freeplay in the pitch control system on the hub forces is negligi-

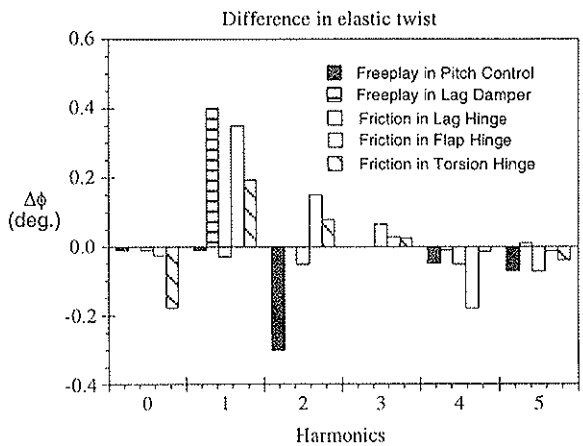

Figure 12: Difference in torsion deflection between undamaged and damaged blades

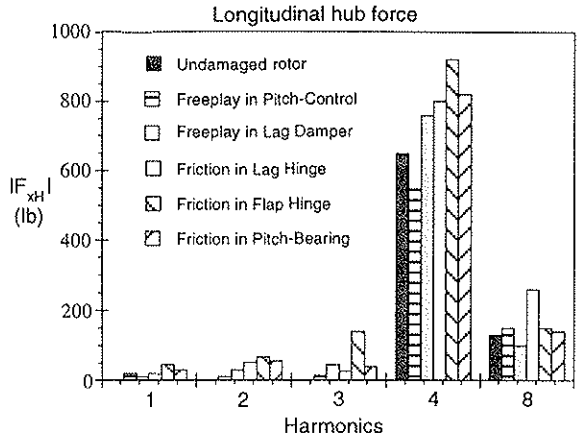

Figure 13: Longitudinal hub force for the undamaged and damaged rotor

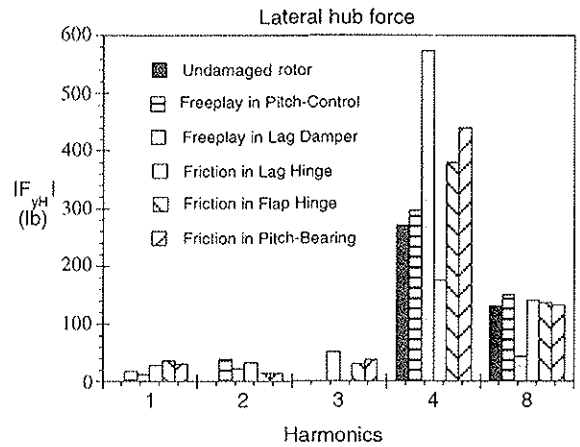

Figure 14: Lateral hub force for the undamaged and damaged rotor

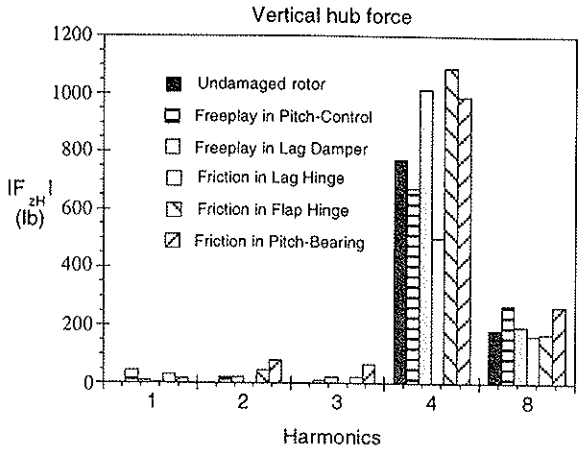

Figure 15: Vertical hub force for the undamaged and damaged rotor

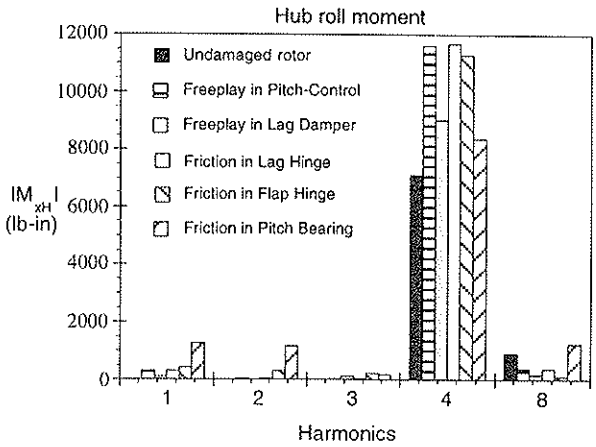

Figure 16: Hub rolling moment for the undamaged and damaged rotor

ble. Freeplay in the lag damper causes a moderate increase in the 4/rev lateral force and a moderate reduction in the 4/rev vertical hub force. The friction in the lag hinge causes a moderate reduction in the 4/rev vertical force. Friction in the flap hinge causes a moderate increase in the 4/rev longitudinal and vertical forces. Friction in the pitch-bearing causes a moderate increase in the 4/rev longitudinal force and a significant increase in the 4/rev vertical force.

Figure 6 shows the diagnostic table for the hub moments. Freeplay in the pitch-control system leads to a moderate increase in the 4/rev rolling and pitching moments. Freeplay in the lag damper causes a moderate increase in the 4/rev pitching moment and a significant increase in the 4/rev yaw moment. Friction in the lag hinge causes a moderate increase in the 4/rev roll moment. Friction in the flap hinge causes a moderate increase in the 4/rev roll and pitch moment and friction in the pitch-control system causes a moderate increase in the 4/rev pitching moment.

It is interesting to note that the changes in the hub loads occur for the 4/rev component primarily for the freeplay and friction faults discussed above.

Faults Used For Damage Detection

Three faults are selected in this study to study the detection of compound faults using neural networks. These are damaged lag damper, damaged pitch control system and moisture absorp-

Table 4: Rotor System Diagnostics in Forward Flight - Blade Tip Response

Damage	Δv	$\angle v$	Δw	$\angle w$	$\Delta \phi$	$\angle \phi$
Free Play in Pitch Control	$\sim$	$\sim$	1-o$^+$	1-◯$^+$	2-o$^-$	$\sim$
Free Play in Lag Damper	$\sim$	$\sim$	$\sim$	$\sim$	1-o$^+$	1-◯$^+$
Friction in Lag Hinge	2-o$^+$	2-o$^-$	1-o$^+$	$\sim$	$\sim$	$\sim$
Friction in Flap Hinge	2-o$^-$	2-◯$^+$	1-o$^+$, 2-o$^-$	$\sim$	1-o$^+$	$\sim$
Friction in Pitch Control System	2-o$^-$	2-o$^-$	0-o$^-$, 1-o$^-$	$\sim$	$\sim$	$\sim$

Table 5: Rotor System Diagnostics in Forward Flight - Hub Forces

Damage	$\lvert \Delta F_{xH} \rvert$	$\angle F_{xH}$	$\lvert \Delta F_{yH} \rvert$	$\angle F_{yH}$	$\lvert \Delta F_{zH} \rvert$	$\angle F_{zH}$
Free Play in Pitch Control	$\sim$	$\sim$	$\sim$	$\sim$	$\sim$	$\sim$
Free Play in Lag Damper	$\sim$	$\sim$	4-o$^+$	4-o$^-$	4-o$^-$	4-o$^-$
Friction in Lag Hinge	$\sim$	$\sim$	$\sim$	$\sim$	4-o$^-$	4-o$^-$
Friction in Flap Hinge	4-o$^+$	$\sim$	$\sim$	$\sim$	4-o$^+$	4-o$^+$
Friction in Pitch Control System	4-o$^+$	$\sim$	$\sim$	$\sim$	4-◯$^+$	4-◯$^+$

Table 6: Rotor System Diagnostics in Forward Flight - Hub Moments

Damage	$\lvert \Delta M_{xH} \rvert$	$\angle M_{xH}$	$\lvert \Delta M_{yH} \rvert$	$\angle M_{yH}$	$\lvert \Delta M_{zH} \rvert$	$\angle M_{zH}$
Free Play in Pitch Control	4-o$^+$	4-o$^-$	4-o$^+$	4-o$^+$	$\sim$	$\sim$
Free Play in Lag Damper	$\sim$	$\sim$	4-o$^+$	4-o$^-$	4-◯$^+$	4-◯$^-$
Friction in Lag Hinge	4-o$^+$	4-◯$^-$	$\sim$	$\sim$	$\sim$	$\sim$
Friction in Flap Hinge	4-o$^+$	4-◯$^+$	4-o$^+$	4-o$^-$	$\sim$	$\sim$
Friction in Pitch Control System	$\sim$	$\sim$	4-o$^+$	4-o$^-$	$\sim$	$\sim$

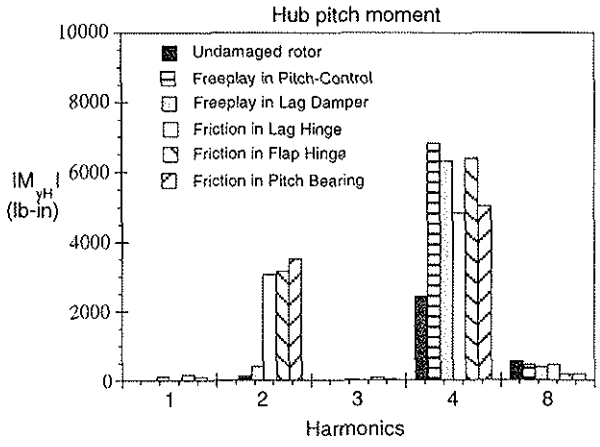

Figure 17: Hub pitching moment for the undamaged and damaged rotor

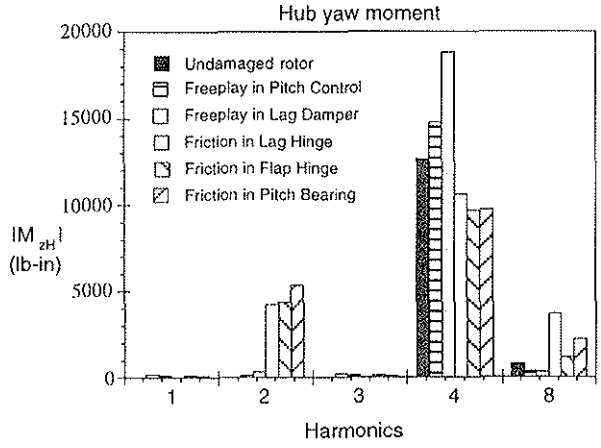

Figure 18: Hub yawing moment for the undamaged and damaged rotor

tion. Several combinations of faults on the damaged blade are also considered.

Number of Neurons Training for both Network A and Network B is started using one neuron in the hidden layer. The number of neurons in the hidden layer is progressively increased from one and the error for generalization of the network is monitored. The error for generalization is defined as

$$e_g = \frac{||t_{test} - t_{output}||}{||t_{test}||} \tag{32}$$

where t_{test} is the desired output and t_{output} is the estimated output of the trained network when presented with test data. The lower the value of e_g, the better the network is at generalizing from training data.

Both ideal and noisy data are used for training and testing the network. All training data is presented to the network simultaneously for all damage levels defined by d_{tr}. Once the network has trained, test data are presented to the trained network simultaneously for all damage levels defined by d_{test}. Both primary and compound faults are considered. The error for generalization is shown in Fig. 19, as the number of neurons in the hidden layer is increased, for Neural Network A and Neural Network B (three combinations of damages). As the number of neurons increases from two, the error for generalization first decreases rapidly and reaches a minimum after which it starts increasing slowly. For Network A, e_g is minimum at 12 neurons and for Network B, around 18 neurons (for three damage combinations). Therefore, Network A and Network B display good generalization characteristics with twelve and eighteen neurons, respectively. Further results in this study use twelve neurons in the hidden layer for Network A and eighteen neurons for Network B.

Damage Detection

Training and Testing Network A is trained using simulated fault data for the three damages over the full range of damage level d_{tr} (Eq. 14). This includes both individual as well as combinations of the damages. Training data for the three damages at damage levels d_{tr} are simultaneously presented to the neural network as matrix P_n. Once the network is trained, the ability of the network to fit the training data exactly is verified. Then, the test data corresponding to damage levels d_{test} (Eq. 15) are analyzed. Both ideal and noise contaminated test data are used. The test data is also simultaneously presented to the trained network for the three damages at damage levels defined by d_{test}. For ideal test data, the network identifies the damage perfectly. Perfect identification im-

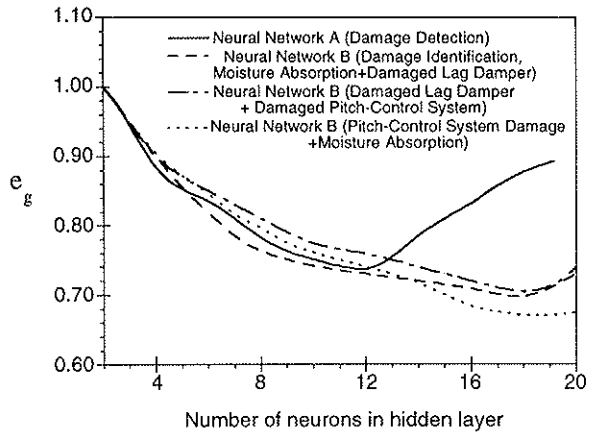

Figure 19: Network error for generalization with increasing number of neurons in hidden layer, normalized by error of generalization with two neurons (all test data presented simultaneously to the trained network)

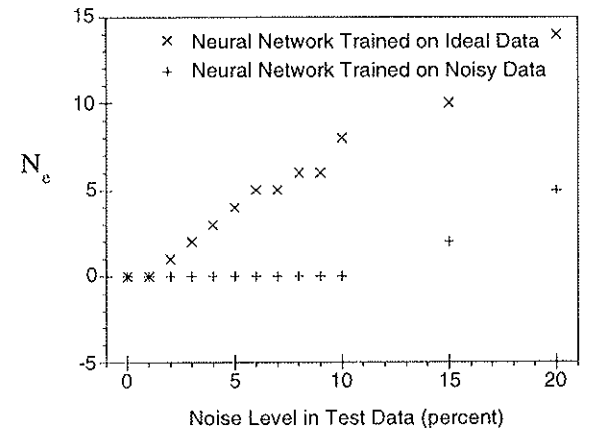

Figure 20: Number of errors in pattern classification with increasing noise level for neural network trained on ideal data and noisy data (all test data presented simultaneously to the trained network)

plies that the target matrix T has the 1's and 0's in the correct places, as shown in Eq. 21.

The trained network is also used to identify damage from noise contaminated data. For noise contaminated test data, the network may make errors as noise levels are increased. As noise levels in the test data are increased, some of the elements of the target matrix are placed into the wrong position by the neural network. The number of errors made by Network A is defined as the number of columns in target matrix T where the 1's and 0's are misplaced, and is denoted by N_e. Fig. 20 shows the number of errors made by the network with increasing noise levels in the test data. For comparison, results from a network trained on ideal data alone are also shown. For a network trained on ideal data alone, it is found that the network begins to misidentify damage even in the presence of low levels of noise (as low as 2 percent) in the test data. However, the network trained on noisy data produces no classification error for noise less than 10 percent and relatively small error at even higher noise levels, compared to the network trained on ideal data alone. This illustrates the benefits of training the neural network using noisy data. Note that the network is trained on noisy data corresponding to five percent and ten percent noise contamination only, for ten cycles.

Reduction in System Parameters used for Training
The neural network uses all 159 rows of the training vector p corresponding to the first five harmonics of the lag, flap and torsion response and the first ten harmonics of the three hub forces and three hub moments. However, many of the elements in p are negligible and it is likely that the neural network makes the pattern classification using only a subset of the system characteristics it receives. To reduce the size of the input vector, the rows of input matrix P and P_n for which all elements are *negligible* are deleted. The definition of *negligible* is given in Table 2. The remaining rows in the input matrix corresponding to system parameters that are *moderate* or *significant*, for at least one damage case, are shown in Table 4. By removing the *negligible* components of the input data, the number of rows in P is reduced from 159 to 70. After deleting the *negligible* system parameters, the network is again trained and tested using the reduced data. The network gives the same results after removal of the negligible inputs, compared to when all inputs are used. This reduced set of network input is used for subsequent results.

Minimum Higher Harmonic System Parameters
To determine the absolute minimum of inputs necessary, each input is eliminated one by one. Higher harmonic inputs are eliminated first. The final

Table 4 - Moderate and Significant Harmonics of System Parameters (per rev)

Δv	Δw	$\Delta\phi$	ΔF_x	ΔF_y	ΔF_z	ΔM_x	ΔM_y	ΔM_z
0	0	3	1	1	1	0	1	0
1	1	4	4	5	2	1	4	4
	3		5	6	3	2	6	5
			6	8	5	4	8	6
			9		8	6		10
			10		10			

Table 5 - Lowest Harmonics of System Parameters Needed for Detection (per rev)

Δv	Δw	$\Delta\phi$	ΔF_x	ΔF_y	ΔF_z	ΔM_x	ΔM_y	ΔM_z
0	0	0	1	1	1	4	1	1
	1	1	4	4	3			4

data set which is able to satisfy training and testing criteria consists of steady lag response, steady and 1/rev flap and torsion response, 1/rev and 4/rev longitudinal and lateral force, 1/rev and 3/rev vertical force, 4/rev rolling moment, 1/rev pitching moment, and 1/rev and 4/rev yawing moments. These system parameters define the lowest harmonics of the system parameters which must be monitored to detect the three damages considered in this study (Table 5). The elements of Table 5 are a subset of the elements in Table 4 and can be used to lower the number of rows in the P matrix from 70 to 26. However, if more damage types are present than the three considered in this study, additional system parameters may have to be monitored.

Sequential Testing The results discussed above were for cases when the neural network was simultaneuosly presented with test data for the three damages at ten damage levels each. This procedure of "batch" or "parallel" testing is useful in determining the network generalization capability and in network sensitivity studies discussed earlier. However, in an actual helicopter, any damage will manifest itself by changes in system parameter vector p corresponding to any one damage at one damage level. The damage detection scheme must be able to detect damage from the input vector p. To simulate this condition, the neural network trained using system parameters in Table 5 is sequentially presented with system response vector p for a given damage at a damage level selected from d_{test}. The correct network output is then a vector t which is {1, 0, 0} for moisture absorption; {0, 1, 0} for lag damper damage; and {0, 0, 1}, for the damaged pitch-control system. If the correct output is obtained when the network is presented with vector p, the network has "detected" the damage. Figures 21, 22 and 23 summarizes the detection results for test data p at several noise levels and damage levels. The shaded squares in these figures indicate successful detection of the damage by the neural network, at a given noise level and damage level. The blank portions of the figure indicate a misdetection.

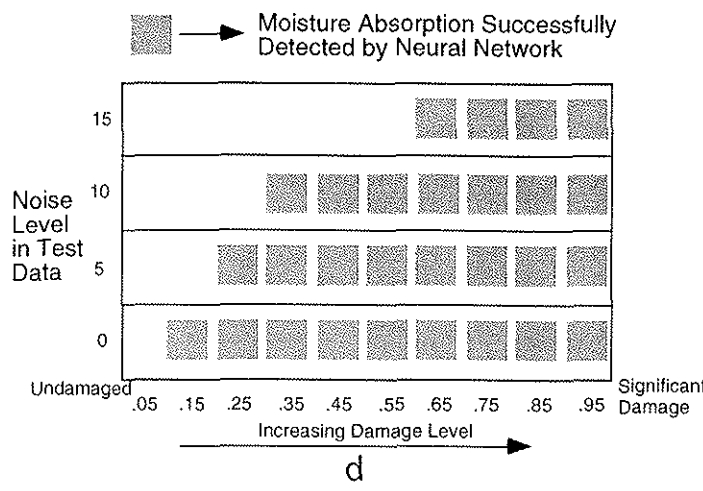

Figure 21: Detection of moisture absorption by trained neural network when sequentially presented with rotor-system response test data at several damage levels

For ideal test data, moisture absorption can be detected for damage level $d \geq 0.15$, and for damaged lag damper and damaged pitch-control system, for

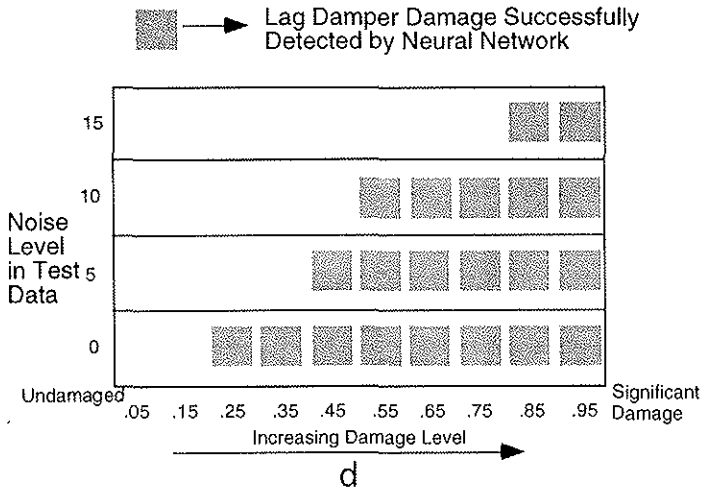

Figure 22: Detection of damaged lag damper by trained neural network when sequentially presented with rotor-system response test data at several damage levels

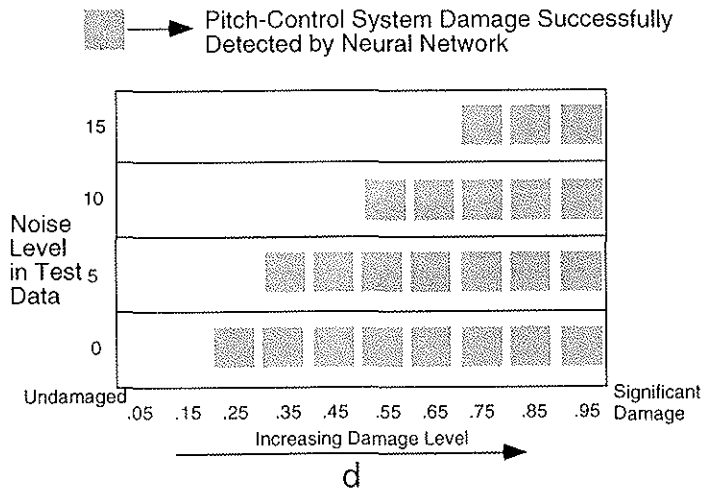

Figure 23: Detection of damaged pitch-control system by trained neural network when sequentially presented with rotor-system response test data at several damage levels

$d \geq 0.25$. As the noise contamination of the test data increases, it becomes progressively difficult for the neural network to correctly detect faults at small damage levels. It appears from these figures that moisture absorption is easier to detect than the other damages, and that faults with high damage levels ($d \geq 0.85$) can be detected even when the system response data has significant noise contamination.

Next, combinations of the faults are investigated. To simulate this condition, the neural network is presented with the system response vector p for two damages at two damage levels. The correct network output is then $\{1, 1, 0\}$ for moisture absorption and damaged lag damper, $\{1, 0, 1\}$ for moisture absorption and damaged pitch control system and $\{0, 1, 1\}$ for damaged lag damper and damaged pitch-control system. If the correct output is obtained when the network is presented with the vector p, the network has detected the damage. Fig. 24 shows the detection resuls at several noise levels and several damage levels for the compound fault consisting of moisture absorption and damaged lag damper. Results are shown for four cases with noise levels in the test data increasing from zero to 15 percent. Successful fault detection by the neural network is represented by the shaded squares shown in the figure. The blank portions in the figure show misdetection. At low noise levels even small damage levels can be detected. However, as the noise level in the test data increases, it becomes difficult to detect damages at small damage levels. Similar results for moisture absorption and damaged pitch control system are shown in Fig. 25 and for damaged lag damper and damaged pitch control system are shown in 26.

Damage Identification

Training and Testing Once the damage has been detected, the next step is damage extent identification, i.e. to estimate the degree of damage. Neural Network B is used for this damage identification. The reduced data set of system parameters shown in Table 5 is used for training and testing the network. The neural network is trained to map the training data to the rotor system parameters corresponding to the damage level d_{tr}. Both ideal and noise contaminated training data are used.

Figures 27-29 shows the identification error varying with the noise level in the test data for three damages. The identification error is defined as

$$e_{id} = \frac{||d_{test} - d_{output}||}{||d_{test}||} \qquad (33)$$

where d_{test} is the desired output of the trained network when exposed to test data and d_{output} is

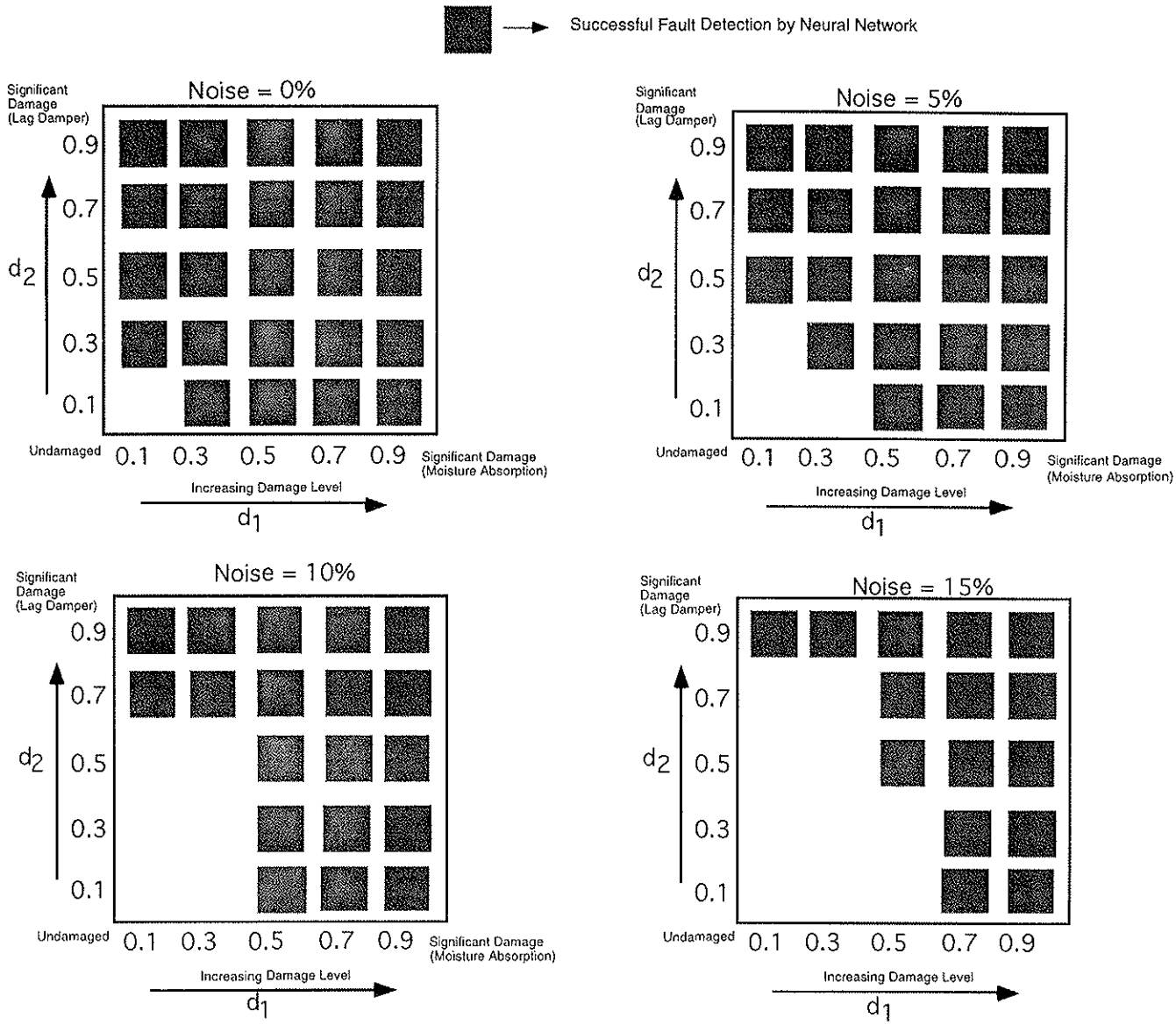

Figure 24: Detection of moisture absorption and damaged lag damper compound fault by trained neural network when sequentially presented with rotor-system response test data at several damage levels and noise levels

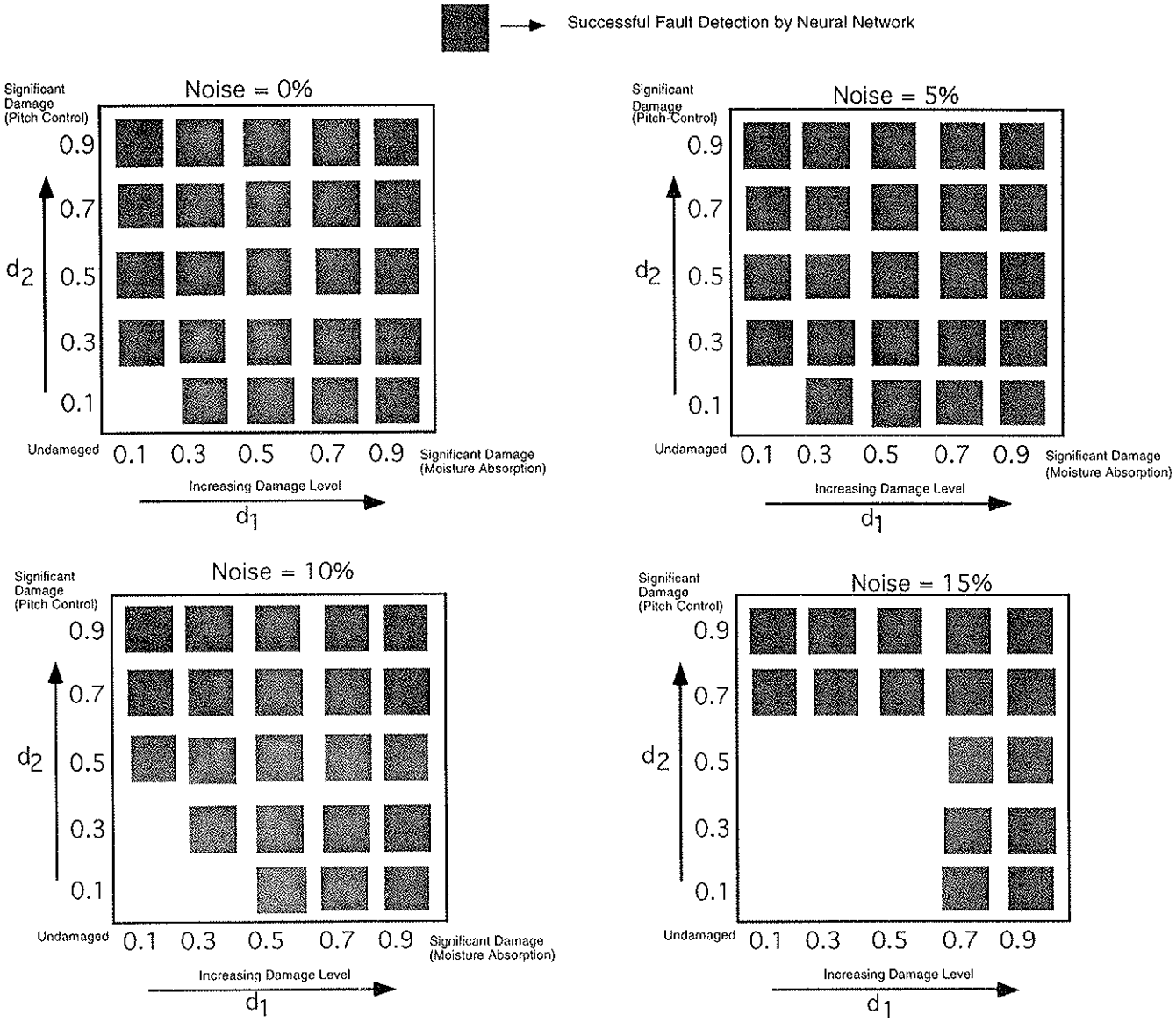

Figure 25: Detection of moisture absorption and damaged pitch-control system compound fault by trained neural network when sequentially presented with rotor-system response test data at several damage levels and noise levels

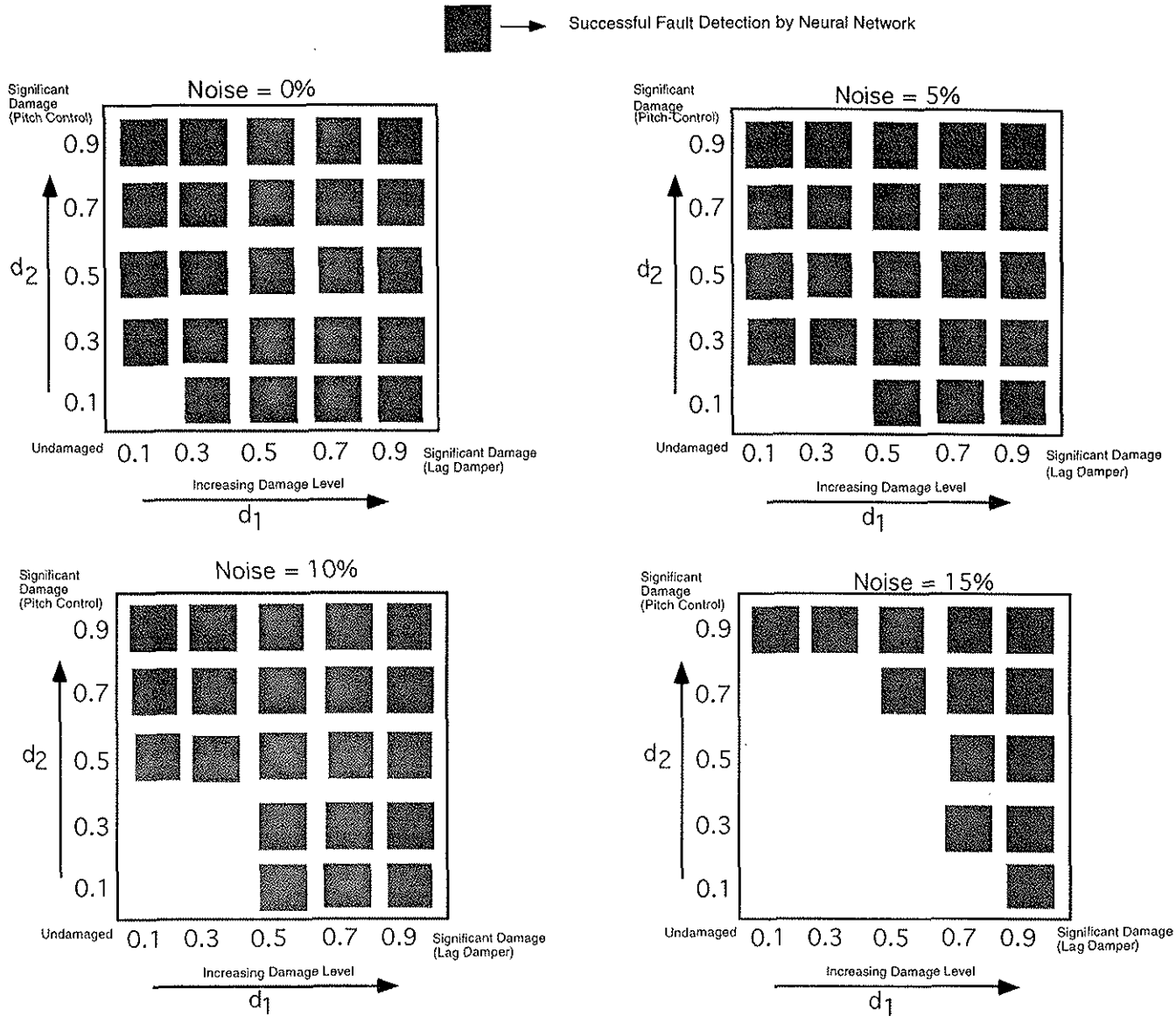

Figure 26: Detection of damaged pitch-control system and damaged lag damper compound fault by trained neural network when sequentially presented with rotor-system response test data at several damage levels and noise levels

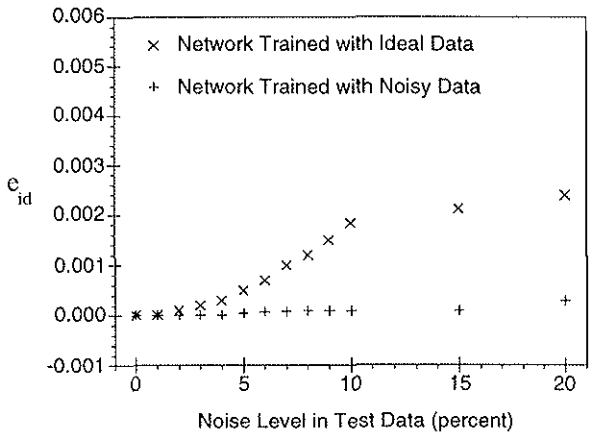

Figure 27: Error in damage identification for moisture absorption with increasing noise level in test data

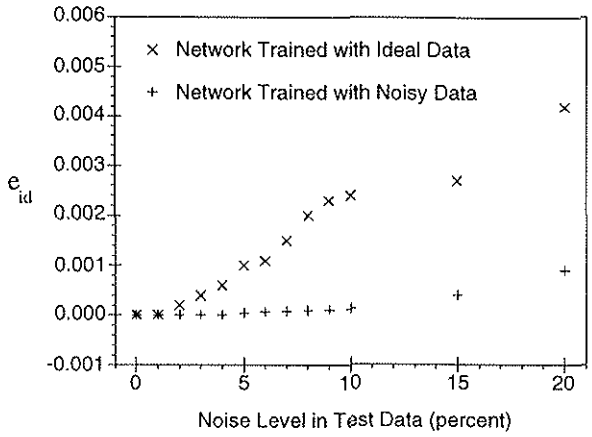

Figure 28: Error in damage identification for damaged lag damper with increasing noise level in test data

the actual output of the network. For comparison, these figures also shows the error of a network trained on ideal data alone. For a noise level below 2 percent, the network trained with ideal data shows zero error. However, as the noise level increases above 2 precent, the network trained on ideal data shows increasing error in identification. The identification error for the network trained with ideal data is relatively higher for the damaged pitch-control system and least for moisture absorption, with the damaged lag damper being in between. In contrast, the network trained on noisy data gives almost zero error for noise levels less that ten percent, and low error even at noise levels of 15 and 20 percent, for all three damages. Note that the noisy training data includes five percent and ten percent noise contamination only, for ten cycles.

Figures 30-32 shows the error in identification of the compound fault consisting of combinations of moisture absorption, damaged lag damper and damaged pitch-control system. In each case, the neural network trained with noisy data gives superior performance compared to the network trained on only ideal data.

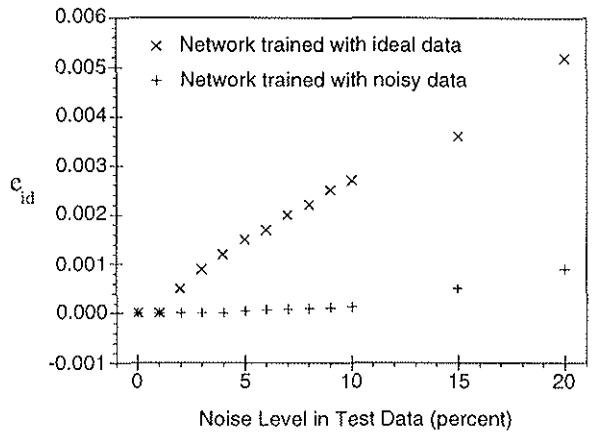

Figure 29: Error in damage identification for damaged pitch-control system with increasing noise level in test data

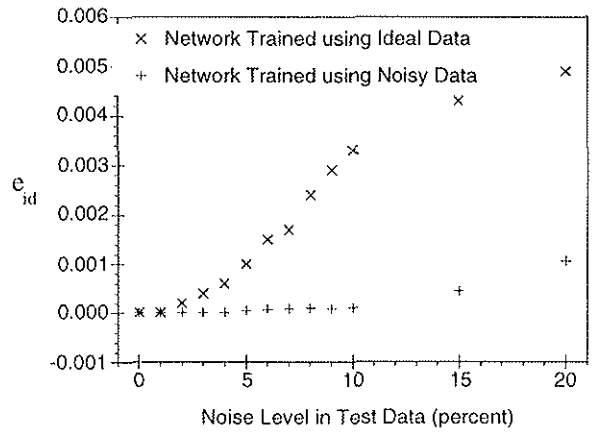

Figure 30: Error in damage identification for moisture absorption and lag damper compound fault with increasing noise level in test data

Conclusions

A physics based model of the helicopter rotor system is used to analyze the influence of selected rotor system faults. Faults modeled include freeplay in the pitch-control system and lag damper and friction in the flap and lag hinges and the pitch control system. In addition, simulated fault data from the damaged rotor system is used to develop a neural network based approach for rotor-system damage detection. Damages used for traing the neural network include moisture absorption, damaged lag damper and damaged pitch-control system. Both single faults and multiple faults are

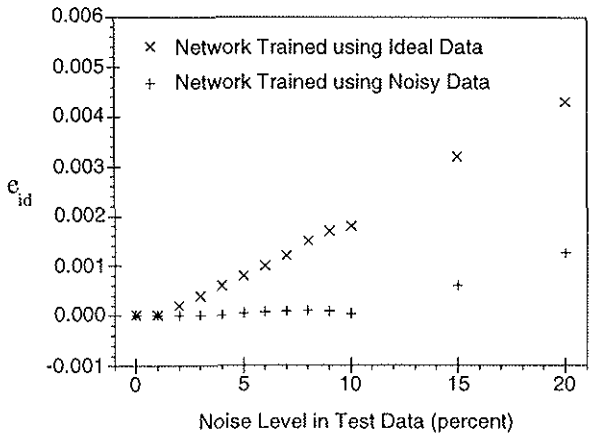

Figure 31: Error in damage identification for moisture absorption and damaged pitch control system compound fault with increasing noise level in test data

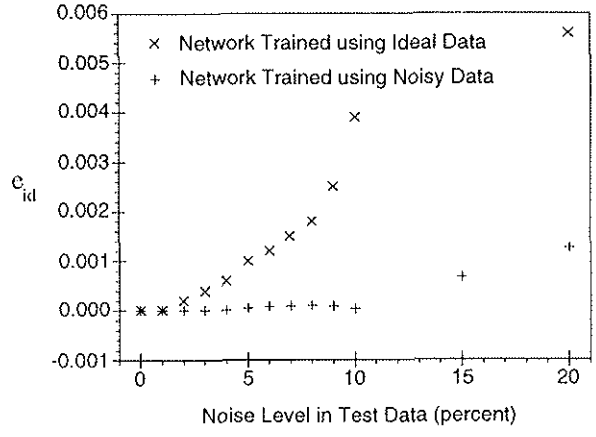

Figure 32: Error in damage identification for damaged lag damper and damaged pitch-control system compound fault with increasing noise level in test data

considered on the damaged blade. The following conclusions are drawn from this study.

1. Freeplay in the pitch control system and the lag damper can be detected by monitoring the 1/rev flap response and the 1/rev and 2/rev torsion response of the damaged blade, and the 4/rev hub loads.

2. Friction in the flap and lag hinge and pitch control system can be detected by monitoring the 2/rev lag response, steady, 1/rev and 2/rev flap response, 1/rev torsion response and 4/rev hub loads.

3. A feedforward neural network using backpropagation learning and one hidden layer can detect and quantify damage after being trained on simulated ideal and noise contaminated data obtained at several damage levels. Damage can be detected for both single faults and multiple faults on the damaged blade.

4. For accurate estimation of the type and extent of damages, it is important to train neural networks with noise contaminated response data. A neural network trained on ideal simulated data shows large errors when even small amount of noise is presented in the test data.

5. For the faults considered in this study a neural network with an input layer, a hidden layer and an output layer is used. The number of neurons in the input and output layers is fixed by the size of the input and output data. For damage detection twelve neurons in the hidden layer are found to be give a low error of generalization. For damage identification, eighteen neurons in the hidden layer is found to give low error of generalization.

6. When the blade tip response, hub forces and hub moments are used together to train the network, damage can be detected without relying significantly on higher harmonic data. For the damages investigated it was found that monitoring the steady lag, flap and torsion response, 1/rev flap and torsion response, 1/rev and 4/rev longitudinal and lateral forces, 1/rev and 3/rev vertical forces, 4/rev rolling moment, 1/rev pitching moment and 1/rev and 4/rev yawing moment data was sufficient for detection and identification.

Acknowledgement

This work was sponsored by the Naval Surface Warfare Center, Carderock Division. The project monitor is Mr. Wayne Boblitt.

References

[1] Land, J., and Weitzman, C., "How HUMS Systems Have the Potential for Significantly Reducing the Direct Operating Costs of Modern Helicopters Through Monitoring", American Helicopter Society 51st Annual Forum, Fort Worth, TX, May 9-11, 1995.

[2] Chronkite, J.D., "Practical Application of Health and Usage Monitoring (HUMS) to Helicopter Rotor, Engine and Drive System", American Helicopter Society 49th Annual Forum, St. Louis, MO, May 19-21, 1993.

[3] Carlson, R.G., Kershner, S.D., and Sewersky, R.A., "Sikorsky Health and Usage Monitoring System (HUMS) Program", American Helicopter Society 52nd Annual Forum, Washington, D.C., June 4-6, 1996.

[4] Cleveland, G. P., and Trammel, C, "An Integrated Health and Usage Monitoring System for the SH-60B Helicopter", American Helicopter Society 52nd Annual Forum, Washington, D.C., June 4-6, 1996.

[5] Azzam, H., and Andrew, M.J., "The Use of Math-Dynamic Models to Aid the Development of Integrated Health and Usage Monitoring Systems," *Journal of Aerospace Engineering*, Part G, Vol. 206, 1992, pp. 71-96.

[6] Ganguli, R., Chopra, I., and Haas, D.J., "Formulation of a Helicopter Rotor-System Damage Detection Methodology," *Journal of the American Helicopter Society*, Vol. 41, No. 4, October 1996.

[7] Ganguli, R., Chopra, I., and Haas, D.J., "Helicopter Rotor-System Damage Detection", Proceedings of the Aeromechanics meeting of the American Helicopter Society, Fairfield County, Connecticut, October 1995.

[8] Bir, G., Chopra, I., Ganguli, R., et al., "University of Maryland Advanced Rotorcraft Code Theory Manual," UM-AERO Report 94-18, July 1994.

[9] Ganguli, R., Chopra, I., and Haas, D.J., "Detection of Simulated Helicopter Rotor System Faults using Neural Networks," Proceedings of the 37th Structures, Structural Dynamics and Materials Conference and Adaptive Structures Forum, Salt Lake City, April 1996.

[10] Haas, D.J., Schaefer, Jr., C.G., "Emerging Technologies for Rotor System Health Monitoring", American Helicopter Society 52nd Annual Forum, Washington, D.C., June 4-6, 1996.

[11] Schoess, J., Malver, F., Iyer, B., Kooyman, J., "Rotor Acoustic Monitoring System (RAMS) - An Application of Acoustic Emission Integrity Monitoring and Assessment", American Helicopter Society 52nd Annual Forum, Washington, D.C., June 4-6, 1996.

[12] Scully, M.P., "Computation of Helicopter Rotor Wake Geometry and its Influence on Rotor Harmonic Airloads,"Massachussetts Institute of Technology, ASRL TR 178-1, Mar 1975.

[13] Leishman, J.G., and Beddoes, T.S., "A Generalized Model for Unsteady Aerodynamic Behavior and Dynamic Stall using the Indicial Method," *Journal of the American Helicopter Society*, Vol. 36, No. 1, Jan 1990.

[14] Haykin, S., *Neural Networks - A Comprehensive Foundation*, Macmillan, 1994.

[15] Vogl, T.P., Mangis, J.K., Rigler, A.K., Zink, W.T., and Alkon, D.L., "Accelerating the Convergence of the Backpropagation Method",*Biological Cybernatics*, Vol. 59, 1988, pp. 257-263.

[16] Nguyen, D., and Widrow, B., "Improving the Learning Speed of a 2-layer Neural Networks By Choosing Initial Values of the Adaptive Weights",International Joint Conference of Neural Networks, Vol. 3, July 1990, pp. 21-26.

[17] Holmstrom, L., and Koistinen, P., "Using Additive Noise in Back Propagation Training", *IEEE Transactions on Neural networks*, Vol. 3, No. 1, Jan. 1992, pp. 24-38.